Available online at www.sciencedirect.com
ScienceDirect
Trans. Nonferrous Met. Soc. China 33(2023) 25−35
Transactions of Nonferrous Metals Society of China
www.tnmsc.cn

Effects of $Al_3(Sc_{1-x}Zr_x)$ nano-particles on microstructure and mechanical properties of friction-stir-welded Al−Mg−Mn alloys

Xin-wen ZHU[1], Ying DENG[1,2], Yi LAI[1], Yi-fan GUO[1], Zi-ang YANG[1], Le FU[1,3], Guo-fu XU[1,2], Ji-wu HUANG[1,2]

1. School of Materials Science and Engineering, Central South University, Changsha 410083, China;
2. State Key Laboratory of Power Metallurgy, Central South University, Changsha 410083, China;
3. Applied Materials Science, Department of Engineering Science, Uppsala University, Uppsala 751 21, Sweden

Received 7 September 2021; accepted 25 February 2022

Abstract: Microstructure and mechanical properties of friction-stir-welded Al−5.50Mg−0.45Mn and Al−5.50Mg−0.45Mn−0.25Sc−0.10Zr (wt.%) alloys were investigated by tensile tests and microscopy methods. The results show that the yield strength, ultimate tensile strength and elongation of the Al−Mg−Mn joint are (191±3) MPa, (315±1) MPa and (4.8±1.9)%, respectively. The corresponding values of the Al−Mg−Mn−Sc−Zr joint are (288±5) MPa, (391±2) MPa and (3.4±1.0)%. The Al−Mg−Mn−Sc−Zr joint has smaller grain size, lower average misorientation angle and higher low-angle grain boundary fraction than the Al−Mg−Mn joint. Both the two joints fracture at the weld nugget zone (WNZ), and $Al_3(Sc_{1-x}Zr_x)$ nano-particles with a mean size of (9.92±2.69) nm still remain in this "weakest zone". Theoretical calculation indicates that nano-particles can provide Orowan and grain boundary strengthening in WNZ, increasing the yield strength of the Al−Mg−Mn joint by 97 MPa.

Key words: aluminum alloy; strength; friction stir welding; nano-particle; microstructure

1 Introduction

Owing to their high strength and good corrosion resistance, Al−Mg alloys are widely used as structural materials in marine and aero-space industry [1]. As an energy efficient and environmentally friendly welding technique, friction stir welding (FSW) technique can achieve high-quality joining of alloys [2−4]. However, due to the heterogeneity of microstructure in friction stir welded joints, the post weld mechanical property is much inferior to that of the base metal. For instance, CHEN et al [5] reported that the ultimate tensile strength of friction-stir-welded 5A06 aluminum alloys was much lower than that of their base metals. A great loss in strength after friction stir welding has been a constraint on the widespread application of 5xxx series alloys and FSW technique.

Currently, improving the performance of the welded alloys is a hot topic. However, the existing reported methods are mainly focused on the post-weld treatment. For instance, THEANO et al [6], KUMAR et al [7] and JIE et al [8] enhance the properties of the welded alloys by the post-weld heat treatment. WILLIAMS et al [9] and KASHANI et al [10] aim at improving the application performance of the weld products by post-weld laser melting and post-weld surface coating. However, these post-weld methods are not suitable for the weld products with large size and high precision requirements. In addition, the post-weld heat treatment is not effective for the non-heat-treatable Al−Mg−Mn welded alloys. Therefore, developing a new pre-weld treatment method for

Corresponding author: Ying DENG, Tel: +86-15974183275, E-mail: csudengying@163.com
DOI: 10.1016/S1003-6326(22)66087-4

improving the properties of the welded products is of great significance in promoting the application of the non-heat-treatable alloys and welding techniques.

Microalloying is an effective approach to improve mechanical properties of aluminum alloys. On a per-atom basis, scandium (Sc) has the greatest strengthening effect among the existing alloying additions to Al [11]. Recent literature and our previous results [12,13] further show that the strength of the aluminum alloys can be substantially improved by adding Sc or Sc and Zr elements. For instance, WU et al [14] reported that the addition of Sc to Al−Cu alloy could induce obvious increments in strength due to the positive effects of the formed Al_3Sc. HUANG et al [15] improve the strength of high-strength aluminum alloys by coherent $Al_3(Sc_{1-x}Zr_x)$ particles. However, there is less effort in improving the strength of the friction stir welded non-heat-treatable Al−Mg−Mn alloys by microalloying or adding $Al_3Sc/Al_3(Sc_{1-x}Zr_x)$ particles. Therefore, in this work, we try to introduce $Al_3(Sc_{1-x}Zr_x)$ particles to the friction stir-welded Al−Mg−Mn alloys by Sc and Zr microalloying and explore the strengthening mechanisms of $Al_3(Sc_{1-x}Zr_x)$ in the welded alloys. It can be expected that this work would offer a new idea for the microstructure and property control of the weld products, and it is of great significance in promoting widespread application of Al−Mg−Mn alloys and friction stir welding processing.

2 Experimental

Semi-continuous alloy ingots, with a diameter of 496 mm, were provided by Northeast Light Alloy Co. Ltd. (China). The nominal chemical compositions of the two kinds of alloy ingots are as follows: Al−5.50Mg−0.45Mn−0.40Si−0.35Fe and Al−5.50Mg−0.45Mn−0.40Si−0.35Fe−0.25Sc−0.10Zr (wt.%), and their measured chemical compositions are Al−5.68Mg−0.47Mn−0.40Si−0.35Fe and Al−5.70Mg−0.45Mn−0.36Si−0.28Fe−0.25Sc−0.10Zr (wt.%). The ingots were homogenized at 440 °C for 12 h in a salt bath furnace, followed by water quenching. Unlike the standard chemical routes for synthesizing discrete nano-particles, $Al_3(Sc_{1-x}Zr_x)$ nano-particles can be formed spontaneously within Al−Mg−Mn−Sc−Zr alloys by controlling micro-alloying composition and processing conditions (homogenization treatment in this study). The homogenized ingots with a dimension of 200 mm × 200 mm × 24 mm, were inter-annealed at 410 °C for 4 h, and then immediately hot-rolled to 6.5 mm-thick plates. Then, the hot-rolled plates were annealed at 420 °C for 1 h, and cold-rolled to 2 mm-thick sheets. To stabilize the microstructure and property of the cold-rolled plates, they were annealed at 300 °C for 1 h. After annealing, the sheets with a dimension of 2 mm × 300 mm × 400 mm were friction stir welded (FSWed) at Beijing FSW Technology Co., Ltd. (China). The welding direction was parallel to the rolling direction of the plates. FSW was performed on a 3 mm gantry milling equipment, using single pass welding. FSW tool is composed of a pin and a shoulder. The pin with a length of 1.75 mm has threaded and its large and small diameters are 3.7 and 3 mm, respectively. The shoulder with a diameter of 14 mm is double-ring-shaped. The tool rotation and the travel speeds were 600 r/min and 200 mm/min, respectively. Under the above processing conditions, the FSWed Al−Mg−Mn alloys can obtain good mechanical properties. The corresponding processing parameters of welds are designed according to our previous works [16−19].

The Vickers hardness measurements were conducted on a HVT−1000A microhardness tester. The load was set as 4.9 N. The mechanical tensile direction was perpendicular to welding direction. Tensile property tests were performed on a CSS−44100 electronic universal testing machine with a loading speed of 2 mm/min. Yield strength of materials was identified at 0.2% plastic strain.

To observe the macrostructure of the welded joints, TD (transverse direction)−ND (normal direction) surface of the joints was ground, polished and finally etched by the Keller solution for 3.5−4.5 min. The Keller solution is composed of 5 mL HNO_3, 2 mL HF, 3 mL HCl and 250 mL distilled water. The etched specimens were observed by using a Leica DMIL LED metalloscope.

Transmission electron microscope (TEM) were applied to observing the microstructure of the welded joints. Thin foils were sectioned from different microstructural zones of the welded alloys and were prepared by double-jet electro-polishing at 20 V in a solution of 30% nitric acid and 70% methanol solution cooled to −30 °C. The thin foils were observed on a TECNAIG^2 20 electron

microscope, with an acceleration voltage of 200 kV. Gatan Digital Micrograph software was used to measure the particle size of $Al_3(Sc_{1-x}Zr_x)$ by (100) supperlattice dark field TEM images. As nano-particles have different sizes, their average size and standard deviation were reported here. To observe the nano-particles, a Titan G^2 60−300 high-resolution aberration-corrected transmission electron microscope, equipped with a high-angle annular-dark-field (HAADF) detector and an X-ray energy dispersive spectrometry (EDS) system, was used at 300 kV for HADDF scanning transmission electron microscopy (STEM) imaging and EDS chemistry STEM (EDXChemi−STEM) analysis.

EBSD (electron back-scattered diffraction) analyses were performed using a Sirion 200 field emission gun scanning electron microscope. EBSD data were analyzed by the OIM Analysis 5 software. In order to avoid spurious boundaries, misorientation angles below 2° were not measured. This limit was used for all samples in order to provide consistent quantitative data. Boundaries with misorientation angles between 2° and 15° were defined as low angle grain boundaries (LAGB) and those of misorientation angle larger than 15° were defined as high angle grain boundaries (HAGB).

3 Results

3.1 Macro metallograph and micro-hardness of joints

The macro metallograph, optical micro-structure, SEM−EDS results and micro-hardness of studied friction stir weld joints are shown in Fig. 1. As the OM images of the two joints are almost the same, only the optical macro-graph of a representative cross section of the Al−Mg−Mn−Sc−Zr alloy weld joints is provided here. The yellow dotted line in Fig. 1(a) is the position for the hardness tests.

Figure 1(a) indicates that the weld joint has the appearance of a classical nugget structure, which shows the material flow pattern as a result of friction stir processing. Besides, the thickness of the whole weld joint is inhomogeneous, and the weld center is the thinnest zone. Moreover, different zones of the FSW weld have different micro-structures (Figs. 1(b−e)). Weld nugget zone (WNZ) shows a fine-grained microstructure and the thermal-mechanical affected zone (TMAZ) is characterized by a highly deformed structure (Fig. 1(d)). Due to the fact that the deformation degree of TMAZ grains at the advancing side is higher, the interface between weld nugget zone and heat-affected zone (HAZ), actually TMAZ, is relatively sharp on the advancing side (Figs. 1(c, e)). The optical microstructure of the HAZ is similar to that of the base alloy (Fig. 1(b)). Hence, the optical microstructures of base metals are not presented here. One dominant characteristic of the Al−Mg−Mn−Sc−Zr welded alloy is that the sizes of the primary $Al_3(Sc_{1-x}Zr_x)$ particles are in micro-scale, which is in accordance with our previous results [19,20] and is identified by SEM−EDS results shown in Figs. 1(f, g). The primary $Al_3(Sc_{1-x}Zr_x)$ particles are distributed in the whole friction stir welded joint, as indicated by the white arrows.

Figure 1(h) shows that the hardness curves of the two welded Al−Mg−Mn sheets both present “W”-like shapes. Compared with the base metals, significant softening can be observed throughout the weld zone, which can be attributed to thermal exposure during friction stir welding process. Combined with the optical microstructure, different microstructural zones of the weld joints can be identified. With the increase of the distance away from the weld center, the hardness values keep stable at first (0−3 mm away from weld center, WNZ), and then decrease sharply to the minimum values (3−4 mm away from the weld center, TMAZ), and finally gradually raise until close to the level of base metal (5−12 mm away from the weld center, HAZ). The interface between the TMAZ and HAZ has the minimum hardness value. Besides, the friction stir-welded Al−Mg−Mn−Sc−Zr alloy has a higher hardness than that of the Al−Mg−Mn welded alloy, including the welding softening zone.

3.2 Mechanical properties

The mechanical properties (yield strength (YS), ultimate tensile strength (UTS), and elongation (El)) of two friction stir-welded alloys are given in Table 1, and their tensile curves are shown in Fig. 2. First, YS, UTS and El of the two welded alloys are all much lower than those of their base metals. This indicates that friction stir welding results in softening of the alloys. Second, FSW welding coefficients (the strength ratio of welded joint to

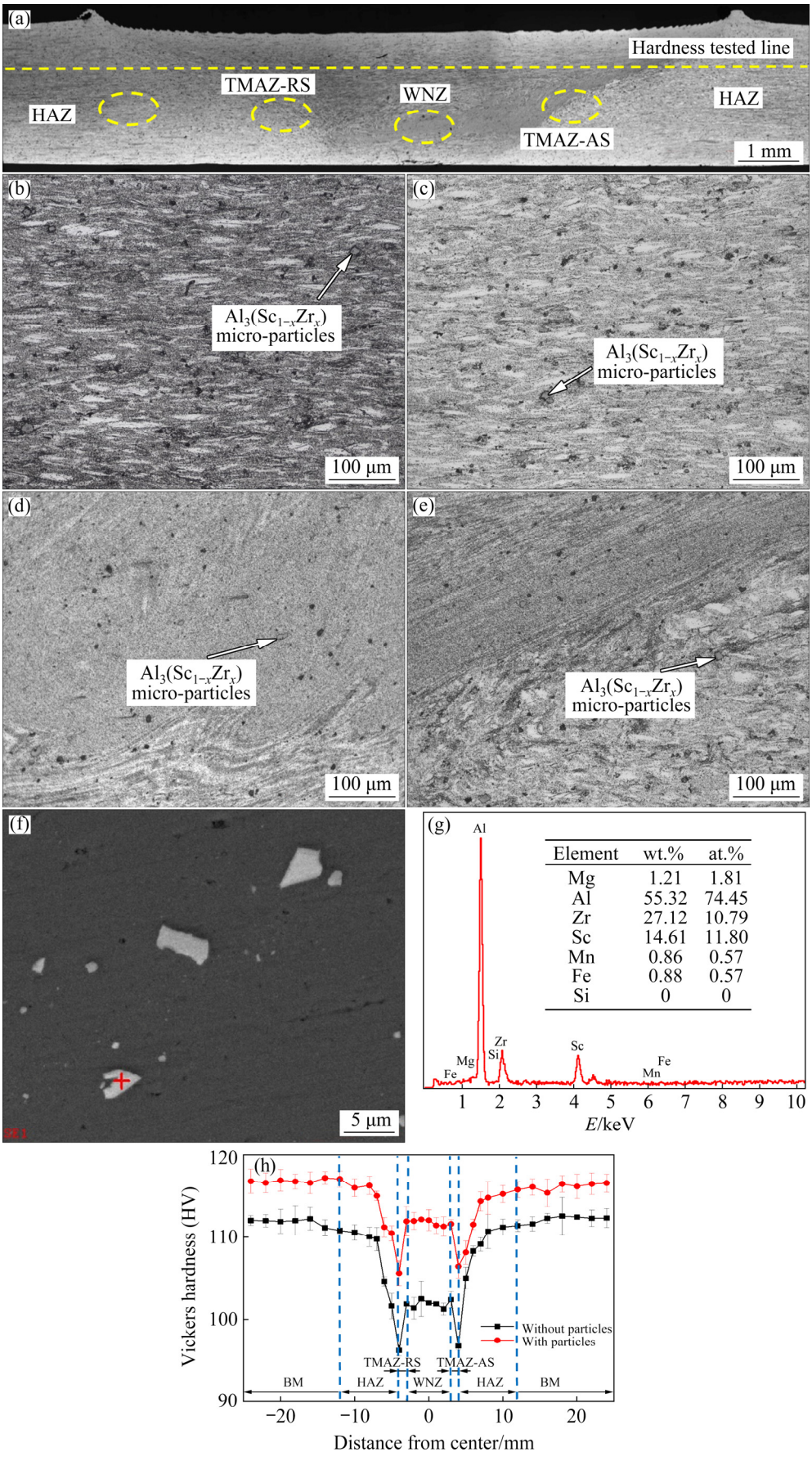

Fig. 1 Macro-structure (a), optical microstructures (b−e), SEM−EDS results (f, g) and micro-hardness (h) of Al−Mg−Mn−Sc−Zr welded alloy: (b) HAZ; (c) TMAZ-RS; (d) WNZ; (e) TMAZ-AS

Table 1 Mechanical properties of two friction stir-welded joints

Alloy	Condition	YS/MPa	UTS/MPa	El/%	Welding coefficient/%
Al−Mg−Mn	Base metal	219±5	364±3	15.7±1.2	93.4±0.4
	Joint	191±3	315±1	4.8±1.9	
Al−Mg−Mn−Sc−Zr	Base metal	313±6	419±3	12.2±2.2	93.9±0.2
	Joint	288±5	391±2	3.4±1.0	

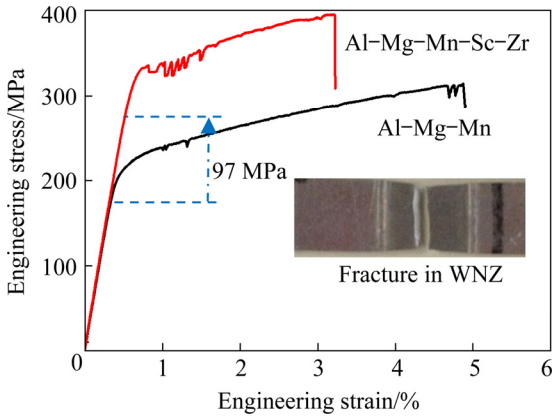

Fig. 2 Tensile curves of friction stir welded joints

base metal) of the two welded alloys are all higher than 93%, showing high-quality joining. Third, Sc and Zr micro-alloying can significantly strengthen the Al−Mg−Mn joints. The YS, UTS and El of the Al−Mg−Mn joint are (191±3) MPa, (315±1) MPa and (4.8±1.9)%, respectively. And, those of the Al−Mg−Mn−Sc−Zr joint are (288±5) MPa, (391±2) MPa and (3.4±1.0)%. Compared with those of the Al−Mg−Mn joints, the YS and UTS of Al−Mg−Mn−Sc−Zr joints are increased by 97 MPa (~51%) and 76 MPa (~24%) (Fig. 2), respectively.

It is worth noting that both the two friction stir welded joints fracture at the weld nugget zone, as demonstrated by the inset in Fig. 2, not at the interface between the HAZ and TMAZ, which has the minimum hardness in the whole joints. This can be explained by the fact that the weld nugget zone is the thinnest part and it shows relatively lower hardness than the other parts.

3.3 Grain and grain boundary characteristics

As the mechanical properties of joints are determined by their "weakest" microstructure zones, the following microstructure characterization is focused on the weld nugget zone. By comparison, microstructures of the base metal (BM) are also characterized. Figure 3 shows the EBSD orientation maps and misorientation angle distributions of BM and WNZ in two welded alloys. The testing plane consists of nominal direction (ND) and rolling direction (RD).

It can be found that the Al−Mg−Mn base metal is characterized by elongated deformed grains and recrystallized grains, while the Al−Mg−Mn−Sc−Zr base metal basically consists of deformed un-recrystallized grains. Lots of sub-grains can be observed in the interior of the deformed grains, and the grain boundaries are characterized by a high fraction of low angle grain boundaries. The welded nugget zones of two joints are composed of equiaxed grains. Due to intense plastic deformation around rotating tool and workpiece and the thermal exposure, the average misorientation angles and the fraction of high angle grain boundaries of weld nugget zones are higher than those of the base metals. By comparing two weld joints, it can be found that the grain sizes, average misorientation angles and fraction of high angle grain boundaries in the Al−Mg−Mn−Sc−Zr joint are all smaller than those of the Al−Mg−Mn joint, revealing that micro-alloying can effectively prevent the occurrence of dynamic recrystallization and the growth of grains during friction stir welding process.

3.4 Substructure and $Al_3(Sc_{1-x}Zr_x)$ nano-particles

Sc and Zr microalloying elements in aluminum alloys mainly exist in the form of $Al_3(Sc_{1-x}Zr_x)$ nano-particles. Figure 4 shows the bright-field TEM image, selected area diffraction pattern, (100) supperlattice dark field image, HAADF-STEM and EDS Chemi-STEM mapping of $Al_3(Sc_{1-x}Zr_x)$ nano-particles in the studied weld joints.

Bright-field TEM images indicate that the BM mainly consist of dislocation tangles (Figs. 4(a, b)) and the WNZ is characterized by substructure or fine subgrains (Figs. 4(e, f)). From BM to WNZ, the increase in HAGBs or the decrease in LAGBs in weld joints is caused by the increase in subgrain sizes or the mergence of subgrains or the grain breaking by friction heat and stirring force during friction stir welding.

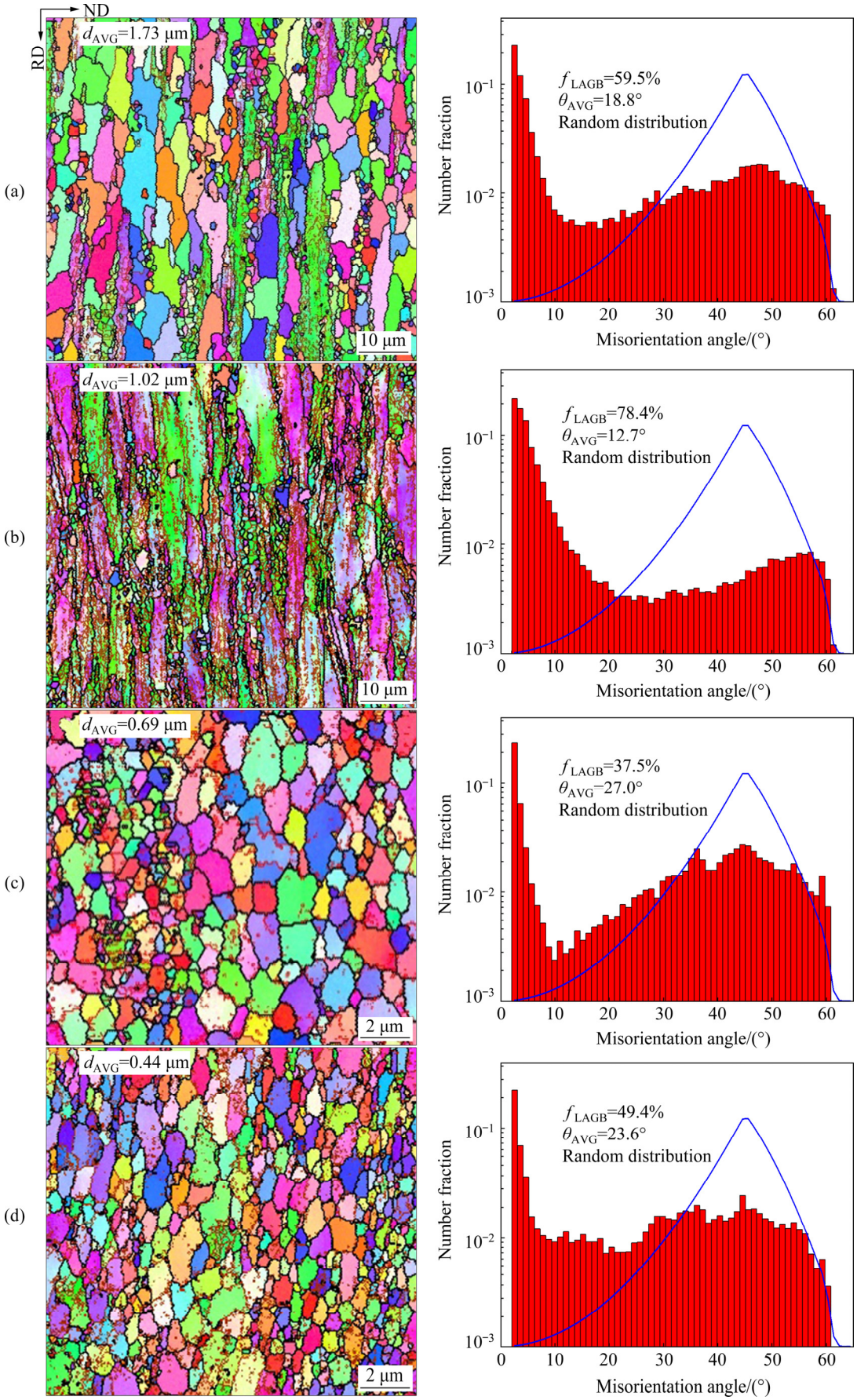

Fig. 3 Orientation maps and misorientation angle distributions of BM and WNZ in two welded alloys: (a) Al−Mg−Mn, BM; (b) Al−Mg−Mn−Sc−Zr, BM; (c) Al−Mg−Mn, WNZ; (d) Al−Mg−Mn−Sc−Zr, WNZ (d_{AVG} is the average grain size)

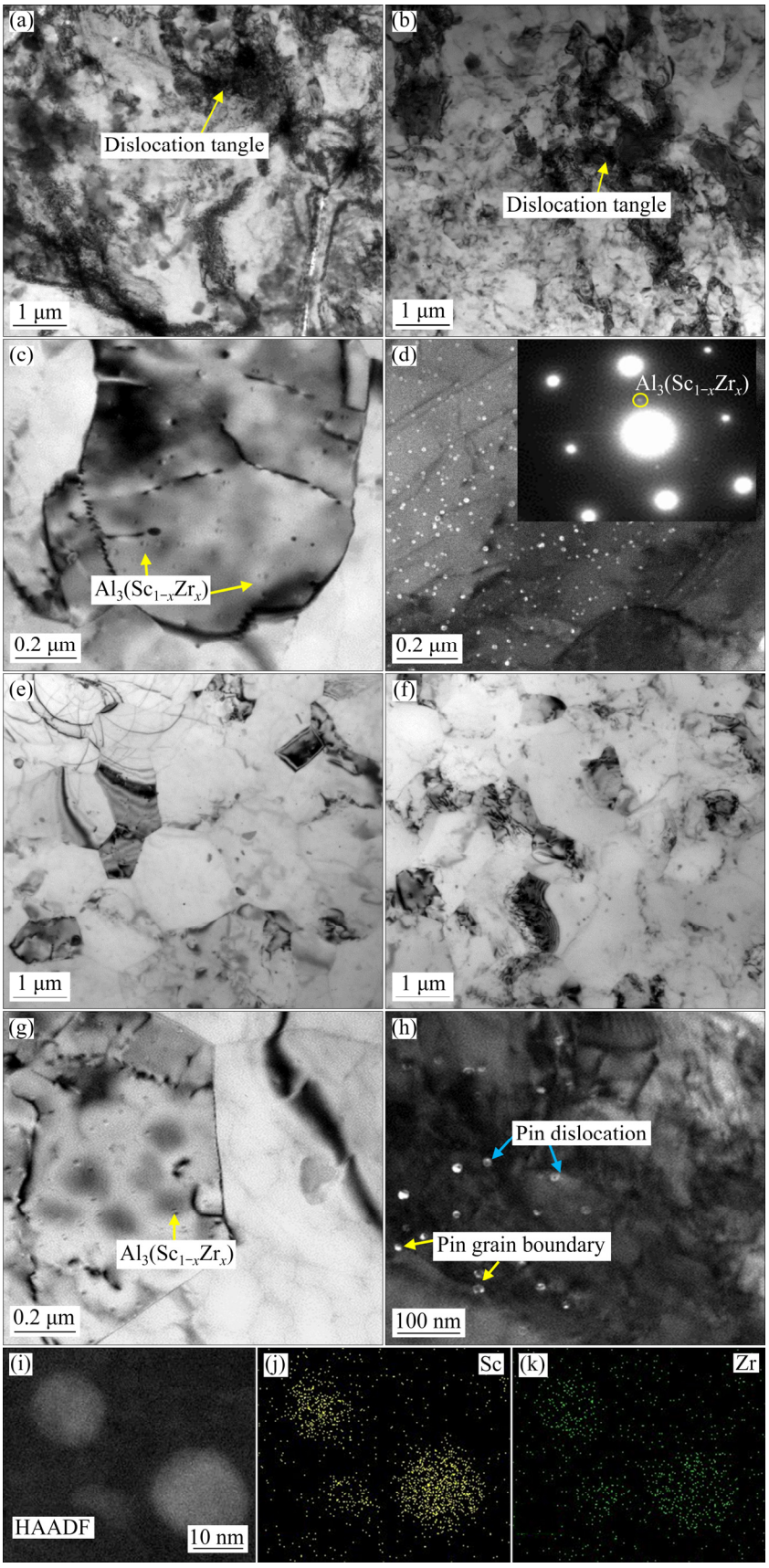

Fig. 4 Bright-field TEM image (a−c, e−g), selected area diffraction pattern (d), (100) supperlattice dark-field image (h), HAADF-STEM (i) and EDS Chemi-STEM mapping (j, k) of $Al_3(Sc_{1-x}Zr_x)$ nano-particles: (a) Al−Mg−Mn, BM; (b−d) Al−Mg−Mn−Sc−Zr, BM; (e) Al−Mg−Mn, WNZ; (f−k) Al−Mg−Mn−Sc−Zr, WNZ

The Al−Mg−Mn−Sc−Zr welded alloy is characterized by a large number of fine secondary particles with Ashby−Brown contrast in the bright-field TEM image (Fig. 4(c)), as well as superstructure reflections like (100) and (110), as shown in the SAD of Fig. 4(d), proving that these spherical particles are $Al_3(Sc_{1-x}Zr_x)$ nano-particles with an $L1_2$ cubic crystal structure and they are coherent with the Al matrix. The $Al_3(Sc_{1-x}Zr_x)$ nano-particles can be found in the whole weld joints, and they have nano-scaled size and show stable coherent relationship with aluminum matrix. Hence, these $Al_3(Sc_{1-x}Zr_x)$ nano-particles can act as an effective pinning site to hinder the migration of grain boundaries and dislocations (Fig. 4(h)). In the weld nugget zone, strong mechanical stirring produces lots of broken grains with high angle grain boundaries, as most of the deformation-induced boundaries have high angle in misorientation. Moreover, due to the intense thermal-mechanical input during friction stir welding, although coherent $Al_3(Sc_{1-x}Zr_x)$ nano-particles exist in the weld nugget zone, partial dynamic recrystallization occurs and the zone has a high fraction of high angle grain boundaries. The compositions of $Al_3(Sc_{1-x}Zr_x)$ nano-particles are further characterized by HAADF-STEM and EDS Chemi-STEM mapping, as shown in Figs. 4(i−k). It can be found that the $Al_3(Sc_{1-x}Zr_x)$ nano-particles mainly consist of Sc and Zr elements. Based on the TEM and EBSD results, it can be concluded that secondary $Al_3(Sc_{1-x}Zr_x)$ nano-particles can effectively prevent grain growth during FSW. This is why the average subgrain sizes of the Al−Mg−Mn−Sc−Zr weld joints are still smaller than those of the Al−Mg−Mn weld joints.

4 Discussion

The minimum hardness values of two friction stir weld joints are both located at the transition zone between HAZ and TMAZ, so the joints are supposed to fracture at this position. However, the thickness in the whole weld joint is inhomogeneous and the weld center is the thinnest zone. In addition, compared with base metal, nugget zone is a softening zone, and the hardness is only slightly higher than that of the minimum value. Therefore, the joints fail at the center of the weld nugget zone during tensile tests.

The strength of weld joints is determined by its "weakest microstructural zone". Therefore, to find out the reason for mechanical property difference between the two studied joints, the effect of $Al_3(Sc_{1-x}Zr_x)$ particles on the microstructure of the weld nugget zone should be discussed.

As mentioned above, $Al_3(Sc_{1-x}Zr_x)$ particles exist in the forms of primary $Al_3(Sc_{1-x}Zr_x)$ micro-particles (Figs. 1) and secondary $Al_3(Sc_{1-x}Zr_x)$ nano-particles (Fig. 4). The former can act as nucleation sites during casting and solidification and refine the grains of cast alloys [21−23]. Therefore, their effect on strength of the friction stir welded alloy can be ignored, due to the fact that the friction stir welding process of aluminum alloy basically can not cause melting and solidification of alloys. As a result, the positive effect from Sc and Zr microalloying on the strength of Al−Mg−Mn weld joint can be predominately attributed to secondary $Al_3(Sc_{1-x}Zr_x)$ nano-particles. These nano-particles can inhibit dynamic recovery or recrystallization during friction stir welding process to prevent the mergence of subgrains and the growth of grains (Figs. 3 and 4), resulting in Hall−Petch or fine-grain strengthening. In addition, the $Al_3(Sc_{1-x}Zr_x)$ nano-particles distributed in high-density can strongly pin dislocations and grain boundaries, providing precipitation strengthening. Precipitation strengthening can generally occur by one of two mechanisms, shearing mechanism or the Orowan strengthening mechanism, depending on the particle size. Transition from the shearing mechanism to Orowan strengthening mechanism occurs when the size of the $Al_3(Sc_{1-x}Zr_x)$ nano-particles is in range of 4−6 nm [24−26]. Hence, the Orowan mechanism should be responsible for the $Al_3(Sc_{1-x}Zr_x)$ particle-induced strengthening in this study, as their average size is about 10 nm.

For better quantitative analyses, the size distribution and number density of $Al_3(Sc_{1-x}Zr_x)$ nano-particles are measured by statistic estimation based on the supperlattice centered dark field TEM images and the results are shown in Fig. 5. It can be seen that friction stir welding processing do not cause a significant coarsening of $Al_3(Sc_{1-x}Zr_x)$ nano-particles, as their size in weld nugget zone ((9.92±2.69) nm) is only slightly larger than that in base metal ((9.76±3.16) nm). This also means that the $Al_3(Sc_{1-x}Zr_x)$ nano-particles have high thermal stability.

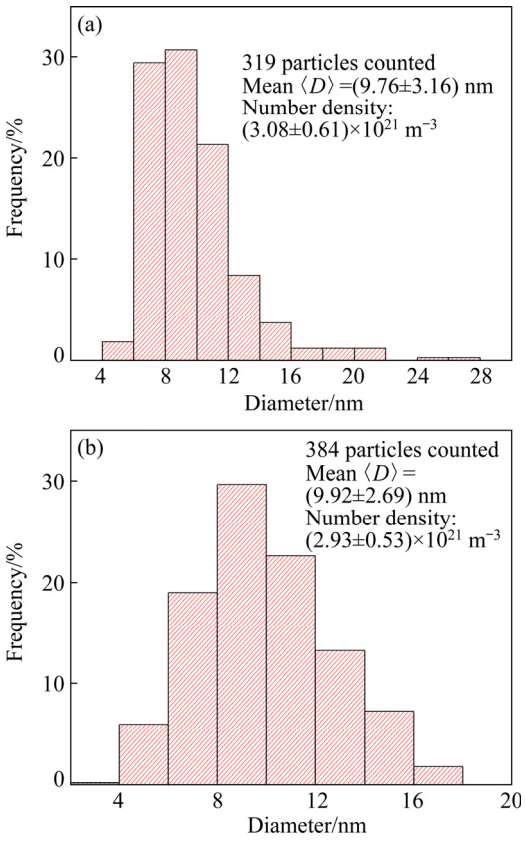

Fig. 5 Size distribution histograms of $Al_3(Sc_{1-x}Zr_x)$ nano-particles: (a) Base metal; (b) Weld nugget zone

4.1 Orowan strengthening

The increase in the YS due to the Orowan strengthening, $\Delta\sigma_{Or}$, is given by [18]

$$\Delta\sigma_{Or} = K_4 M(1-\nu)^{-0.5}(Gb/\lambda)\ln(d_s/b) \quad (1)$$

$$d_s = \frac{\pi d_m}{4} \quad (2)$$

$$\lambda = \left[\frac{1}{2}\left(\frac{2\pi}{3f_V}\right)^{0.5} - 1\right]\frac{\pi d_m}{4} \quad (3)$$

where M is the Taylor factor; ν and G are Poisson's ratio and the shear modulus of the matrix, respectively; b is the magnitude of Burgers vector of the Al matrix, K_4 is a constant; d_s and λ are the mean particle diameter and an effective inter-particle distance, respectively; d_m and f_v are the size and volume fraction of $Al_3(Sc_{1-x}Zr_x)$ particles, respectively. The following values are used to calculate $\Delta\sigma_{Or}$: K_4=0.127, M=3.06, ν=0.331, G=27.8 GPa, and b=0.286 nm. The additional Orowan strength in the weld nugget zone related to the $Al_3(Sc_{1-x}Zr_x)$ nano-particles is calculated as 90.7 MPa.

4.2 Grain boundary strengthening (Hall–Petch)

The standard Hall−Petch equation, Eq. (4), is employed to relate the yield strength of the material (σ) to the average grain size (d):

$$\sigma_{H-P} = \sigma_0 + kd^{-1/2} \quad (4)$$

where σ_0 is the intrinsic resistance of the lattice to dislocation motion and k is a parameter that describes the relative strengthening contribution of grain boundaries. The k value of 0.04 MPa·m$^{1/2}$ for aluminum [27,28] is used to estimate the strengthening due to grain boundaries.

The increase in the YS due to the grain boundary strengthening from $Al_3(Sc_{1-x}Zr_x)$ nano-particles, $\Delta\sigma_{H-P}$, is given as follows:

$$\Delta\sigma_{H-P} = k(d^{-1/2}_{\text{with particles}} - d^{-1/2}_{\text{without particles}}) \quad (5)$$

By substituting k value and grain sizes in the weld nugget zone of two studied friction stir welded joints, $\Delta\sigma_{H-P}$ related to the $Al_3(Sc_{1-x}Zr_x)$ nano-particles in weld nugget zone is calculated as 9.0 MPa .

Therefore, the calculated YS increment in Al−Mg−Mn joints contributed by $Al_3(Sc_{1-x}Zr_x)$ nano-particles is about 99.7 MPa in the weld nugget zone, which is very close to the experimental result of 97 MPa. Moreover, it can be concluded that the improved strength of Al−Mg−Mn friction stir welded joints can be attributed to Orowan strengthening of $Al_3(Sc_{1-x}Zr_x)$ nano-particles.

5 Conclusions

(1) Friction stir-welded Al−Mg−Mn−Sc−Zr alloy has higher hardness than Al−Mg−Mn welded alloy. The minimum hardness values of two welded joints locate at the interface between the thermal-mechanical affected zone and heat affected zone.

(2) The yield strength, ultimate tensile strength and elongation to failure of the Al−Mg−Mn joint are (191±3) MPa, (315±1) MPa and (4.8±1.9)%, respectively. And the corresponding values of the Al−Mg−Mn−Sc−Zr joint are (288±5) MPa, (391±2) MPa and (3.4±1.0)%, respectively.

(3) The Al−Mg−Mn−Sc−Zr joint has smaller grain size, lower average misorientation angle and higher low angle grain boundary fraction than the Al−Mg−Mn joint.

(4) Two studied joints both fracture at the weld

nugget zone during tensile tests. $Al_3(Sc_{1-x}Zr_x)$ nano-particles with a mean size of (9.92±2.69) nm remain in this "weakest zone". These nano-particles can provide Orowan strengthening and grain/subgrain boundary strengthening in the weld nugget zone, increasing the yield strength of Al−Mg−Mn joints by 97 MPa (~51%). Theoretical calculations further reveal that Orowan strengthening is the dominant strengthening mechanism of $Al_3(Sc_{1-x}Zr_x)$ nano-particles in friction stir weld joints.

Acknowledgments

This work was financially supported by the Natural Science Foundation of Hunan Province, China (Nos. 2020JJ4114, 2016JJ3151), the National Natural Science Foundation of China (No. 51601229), the Young Elite Scientist Sponsorship Program by CAST, China (No. 2015QNRC001), the Hunan Province Innovation Platform and Talent Plan, China (No. 2015RS4001), and the Open-End Fund for the Valuable and Precision Instruments of Central South University, China (No. CSUZC201815).

References

[1] USSAIN G, ILYAS M, LEMOPI ISIDORE B B, KHAN W A. Mechanical properties and microstructure evolution in incremental forming of AA5754 and AA6061 aluminum alloys [J]. Transactions of Nonferrous Metals Society of China, 2020, 31: 51−64.

[2] QIN Q D, ZHAO H L, LI J, ZHANG Y Z, SU X D. Microstructure and mechanical properties of friction stir processed $AlMg_2Si$ alloys [J]. Transactions of Nonferrous Metals Society of China, 2020, 30: 2355−2368.

[3] VYSOTSKIY I, ZHEMCHUZHNIKOVA D, MALOPHEYEV S, MIRONOV S, KAIBYSHEV R. Microstructure evolution and strengthening mechanisms in friction-stir welded Al−Mg−Sc alloy [J]. Materials Science and Engineering A, 2019, 770: 138540.

[4] YANG C, ZHANG J F, MA G N, WU L H, ZHANG X M, HE G Z, XUE P, NI D R, XIAO B L, WANG K S, MA Z Y. Microstructure and mechanical properties of double-side friction stir welded 6082Al ultra-thick plates [J]. Journal of Materials Science & Technology, 2020, 41: 105−116.

[5] CHEN S J, LI X X, JIANG X Q, YUAN T, HU Y Z. The effect of microstructure on the mechanical properties of friction stir welded 5A06 Al alloy [J]. Materials Science Engineering A, 2018, 735: 382−393.

[6] THEANO N E, NIKOLAI K, VOLKER V, BENJAMIN K, NIKOLAOS D A. Effect of filler wire and post weld heat treatment on the mechanical properties of laser beam-welded AA2198 [J]. Materials Characterization, 2021, 178: 111257.

[7] KUMAR S D, KUMAR S S. Effect of heat treatment conditions on ballistic behaviour of various zones of friction stir welded magnesium alloy joints [J]. Transactions of Nonferrous Metals Society of China, 2021, 31: 156−166.

[8] JIE Y I, WANG G, LI S K, LIU Z W, GONG Y L. Effect of post-weld heat treatment on microstructure and mechanical properties of welded joints of 6061-t6 aluminum alloy [J]. Transactions of Nonferrous Metals Society of China, 2019, 29: 2035−2046.

[9] WILLIAMS S W, AMBAT R, PRICE D, JARIYABOON M, WESCOTT A. Laser treatment method for improvement of the corrosion resistance of friction stir weld [J]. Materials Science Forum, 2003, 426/427/428/429/430/431/432: 2855−2860.

[10] KASHANI H, AMADEH A, GHASEMI H M. Room and high temperature wear behaviors of nickel and cobalt base weld overlay coatings on hot forging dies [J]. Wear, 2007, 262: 800−806.

[11] YANG C, CAO L F, GAO Y H, CHENG P M, ZHANG P, KUANG J, ZHANG J Y, LIU G, SUN J. Nanostructural Sc-based hierarchy to improve the creep resistance of Al−Cu alloys [J]. Materials & Design, 2020, 186: 108309.

[12] VYSOTSKIY I, KIM K, MALOPHEYEV S, MIRONOV S, KAIBYSHEV R. Superplastic behavior of friction-stir welded Al−Mg−Sc−Zr alloy in ultrafine-grained condition [J]. Transactions of Nonferrous Metals Society of China, 2022, 32: 1083−1095.

[13] DENG Y, YIN Z M, ZHAO K, DUAN J Q, HU J, HE Z B. Effects of Sc and Zr microalloying additions and aging time at 120 °C on the corrosion behaviour of an Al−Zn−Mg alloy [J]. Corrosion Science, 2012, 65: 288−298.

[14] WU S H, ZHANG P, SHAO D, CHENG P M, KUANG J, WU K, ZHANG J Y, LIU G, SUN J. Grain size-dependent Sc microalloying effect on the yield strength-pitting corrosion correlation in Al−Cu alloys [J]. Materials Science Engineering A, 2018, 721: 200−214.

[15] HUANG J W, ZHU X W, LAI Y, GUO Y F, XU G F, ZHANG G, DENG Y. Mechanisms of improving strength and corrosion resistance of high-strength aluminum alloy bars by coherent $Al_3(Sc_{1-x}Zr_x)$ particles [J]. The Chinese Journal of Nonferrous Metals, 2021, 31(6): 1436−1451. (in Chinese)

[16] PENG Y Y, LI S, DENG Y, ZHOU H, XU G F, YIN Z M. Synergetic effects of Sc and Zr microalloying and heat treatment on mechanical properties and exfoliation corrosion behavior of Al−Mg−Mn alloys [J]. Materials Science Engineering A, 2016, 666: 61−71.

[17] DENG Y, PENG B, XU Gu F, PAN Q L, YIN Z M, YR R, WANG Y J, LU L Y. Effects of Sc and Zr on mechanical property and microstructure of tungsten inert gas and friction stir welded aerospace high strength Al−Zn−Mg alloys [J]. Materials Science Engineering A, 2015, 639: 500−513.

[18] DENG Y, YIN Z M, XU G F. Microalloying in Al−Zn−Mg series alloys [M]. Changsha: Central South University Press, 2015. (in Chinese)

[19] DENG Y, ZHANG G, YANG Z A, XU G F. Microstructure characteristics and mechanical properties of new aerospace Al−Mg−Mn alloys with $Al_3(Sc_{1-x}Zr_x)$or $Al_3(Er_{1-x}Zr_x)$ nanoparticles [J]. Materials Characterization, 2019, 153: 79−91.

[20] DENG Y, YIN Z M, ZHAO K, DUAN J Q, HE Z B. Effects of Sc and Zr microalloying additions on the microstructure and mechanical properties of new Al−Zn−Mg alloys [J]. Journal of Alloys and Compounds, 2012, 530: 71−80.
[21] DAVYDOV V G, ELAGIN V I, ZAKHAROV V V, ROSTOVA T D. Alloying aluminum alloys with scandium and zirconium additives [J]. Metal Science and Heat Treatment, 1996, 38: 347−352.
[22] MA R L, PENG C Q, CAI Z Y, WANG R C, ZHOU Z H, LI X P, CAO X Y. Finite element analysis of temperature and stress fields during the selective laser melting process of Al−Mg−Sc−Zr alloy [J]. Transactions of Nonferrous Metals Society of China, 2021, 31: 2922−2938.
[23] CAVALIERE P, CABIBBO M. Effect of Sc and Zr additions on the microstructure and fatigue properties of AA6106 produced by equal-channel-angular-pressing [J]. Materials Characterization, 2008, 59: 197−203.
[24] SENKOV O N, SHAGIEV M R, SENKOVA S V, MIRACLE D B. Precipitation of Al_3(Sc,Zr) particles in an Al−Zn−Mg−Cu−Sc−Zr alloy during conventional solution heat treatment and its effect on tensile properties [J]. Acta Materialia, 2008, 56: 3723−3738.
[25] KENDIG K L, MIRACLE D B. Strengthening mechanisms of an Al−Mg−Sc−Zr alloy [J]. Acta Materialia, 2002, 50: 4165−4175.
[26] FULLER C B, SEIDMAN D N, DUNAND D C. Mechanical properties of Al(Sc, Zr) alloys at ambient and elevated temperatures [J]. Acta Materialia, 2003, 51: 4803−4814.
[27] HANSEN N. Hall−Petch relation and boundary strengthening [J]. Scripta Materialia, 2004, 51: 801−806.
[28] GU G L, KE X N, HU F P, ZHAO S J, WEI G B, YANG Y, PENG X D, XIE W D. Fine-grained Mg−1Mn−0.5Al−0.5Ca−0.5Zn alloy with simultaneously high strength and good ductility fabricated by conventional extrusion [J]. Transactions of Nonferrous Metals Society of China, 2022, 32: 483−492.

$Al_3(Sc_{1-x}Zr_x)$纳米粒子对搅拌摩擦焊 Al−Mg−Mn 合金显微组织和力学性能的影响

朱鑫文[1]，邓 英[1,2]，赖 毅[1]，郭一帆[1]，杨子昂[1]，傅 乐[1,3]，徐国富[1,2]，黄继武[1,2]

1. 中南大学 材料科学与工程学院，长沙 410083；
2. 中南大学 粉末冶金国家重点实验室，长沙 410083；
3. Applied Materials Science, Department of Engineering Science, Uppsala University, Uppsala 751 21, Sweden

摘 要：通过拉伸测试和显微分析方法研究搅拌摩擦焊 Al−5.50Mg−0.45Mn 和 Al−5.50Mg−0.45Mn−0.25Sc−0.10Zr(质量分数，%)合金的显微组织和力学性能。结果表明，Al−Mg−Mn 接头的屈服强度、抗拉强度和伸长率分别为(191±3) MPa、(315±1) MPa 和(4.8±1.9)%，Al−Mg−Mn−Sc−Zr 接头的分别为(288±5) MPa、(391±2) MPa 和(3.4±1.0)%。相比 Al−Mg−Mn 接头，Al−Mg−Mn−Sc−Zr 接头晶粒更细小、平均取向差角更低、小角度晶界百分数更高。两种接头的断裂位置均位于焊核区(WNZ)，在该“最薄弱微区”内，$Al_3(Sc_{1-x}Zr_x)$纳米粒子的平均尺寸为(9.92±2.69) nm，可提供有效奥罗万和晶界强化，使 Al−Mg−Mn 接头的屈服强度提高 97 MPa。

关键词：铝合金；强度；搅拌摩擦焊；纳米粒子；显微组织

(Edited by Bing YAN)